Journal of Cleaner Production 332 (2022) 130095

Contents lists available at ScienceDirect

Journal of Cleaner Production

journal homepage: www.elsevier.com/locate/jclepro

A renewable admixture to enhance the performance of cement mortars through a pre-hydration method

Yi Fang [a], Jialai Wang [a,*], Xin Qian [b], Liang Wang [c,a], Peiyuan Chen [c], Pizhong Qiao [d]

[a] Department of Civil, Construction, and Environmental Engineering, The University of Alabama, Tuscaloosa, AL, 35487, United States
[b] Key Laboratory of Infrastructure Durability and Operation Safety in Airfield of CAAC, Tongji University, Shanghai, 201804, PR China
[c] School of Civil Engineering and Architecture, Anhui University of Science and Technology, Huainan, 232001, Anhui, PR China
[d] School of Naval Architecture, Ocean and Civil Engineering, Shanghai Jiao Tong University, Shanghai, China

ARTICLE INFO

Handling Editor: Zhen Leng

Keywords:
Tannic acid
Renewable admixture
In-situ production
Nanoparticles
Microstructure
Eco-efficiency

ABSTRACT

Aiming to reduce the carbon emission associated with ordinary Portland cement (OPC) based cementitious materials, this study explores a ubiquitous biomolecule, Tannic Acid (TA) to enhance the eco-efficiency of cement mortars through a pre-hydration process. To this end, a small amount of cement is first hydrated in the presence of TA. Due to multiple interactions between the TA and the hydration products of cement, nanoparticles are in situ produced and well-dispersed in the produced cement slurry, which is then used to mix cement mortar. The filler effect of these nanoparticles, together with the dispersing effect of the residual TA in the slurry, can improve the particle packing of the mortar, leading to significant enhancement on the mechanical properties of the produced mortars. Aiming to understand the underlying working mechanisms of the proposed method, a comprehensive experimental program was carried out to characterize the produced nanoparticles and evaluate the effects of the proposed method on the hydration kinetics, workability, setting time, compressive strength, pore structure, and nanomechanical properties of the cement mortar. Testing results show that the proposed method alters the hydration kinetic, increases in the workability of the mortar by up to 7.58%, and reduces the porosity of the cement pastes by more than 17.50%. As a result, the proposed method improves the compressive strengths of the mortars at 180d by up to 45%, significantly enhancing the eco-efficiency of the produced mortars. This study opens news routs and creates new opportunities to identify and design a new generation of chemical admixtures. Unlike traditional, nonrenewable fossil carbon-based admixtures, the new admixtures are renewable, low-cost, and nontoxic.

1. Introduction

Concretes with ordinary Portland cement (OPC) as the binder are the most used construction material in the world. However, the production of OPC is responsible for approximately 8% of anthropogenic greenhouse gas emissions (Kajaste and Hurme, 2016). One effective strategy to reduce the greenhouse gas emissions associated with concretes is to enhance the strength and durability of the concrete so that less cement and concrete are needed. Traditionally, the strength of concretes can be improved by using more binders and maximizing the packing density of aggregates. This usually leads to higher carbon emission. This study hypothesizes that small-dose molecular-scale admixtures can drastically enhance the performance of ordinary Portland cement (OPC) concrete without using any extra cement.

The objective of this study is to identify such an admixture, which can be used in concrete as either a strength (as a performance indicator) enhancer or a cement reducer. When used as the strength enhancer, it can greatly improve the strength of the concrete without using more cement, so that the total amount of concrete required for a specific construction process is reduced. When used as a cement reducer, it can significantly reduce the amount of cement needed for the concrete to achieve a targeted strength. Either way, the total amount of OPC needed for a construction project is reduced.

Highly specific surface interactions is a prerequisite to tune the properties of concretes. Although many chemical admixtures exist for concretes, their reactivities are limited. More importantly, most existing chemical admixtures are synthesized from petroleum derivatives, a nonrenewable resource. Some of them can have toxic long-term effects

* Corresponding author.
E-mail address: jwang@eng.ua.edu (J. Wang).

https://doi.org/10.1016/j.jclepro.2021.130095
Received 26 July 2021; Received in revised form 17 November 2021; Accepted 11 December 2021
Available online 15 December 2021

such as the creation of formaldehydes (Zhang et al., 2008).

Believing in that "Nature has solution to every problem", we turn to naturally occurring materials, mainly bio-based materials, for new admixtures to significantly enhance the performance of concretes (Yan et al., 2020, 2021). This new class of bio-based admixtures broaden the range and possibilities of traditional petroleum-based admixtures used in existing studies and offer higher specificity for interaction with targeted cement phases. More importantly, these nature origin admixtures are inherently sustainable. They are abundant, renewable, low/negative carbon, yet low-cost.

In this study, tannic acid (TA) is identified as such an admixture for its unique chemical structure. With abundant reactive terminal phenolic hydroxyl groups, TA has an ability to complex or cross-link macromolecules sites through multiple interactions, including hydrogen bonding, electrostatic interaction, covalent bonding, and noncovalent interactions (Erel-Unal and Sukhishvili, 2008; Guo et al., 2021; Shutava et al., 2005). In addition, the polyphenol groups have ability to capture metal ions like Ca^{2+}, Fe^{3+}, and Al^{3+} etc., due to the formation of metal-polyphenol coordination (Ren et al., 2021). Due to the π-π stacking of planar aromatic nucleuses in TA, hydrophobic interaction exists between TA and the substrate molecules, which will generate steric repulsion and provide better dispersion (Du et al., 2021). TA can be extracted from many plant parts (Arbenz and Avérous, 2015) and even be made from current industrial waste and byproducts (Arvanitoyannis et al., 2006; Balasundram et al., 2006). As a result, TA can be obtained at around $1/kg (Arbenz and Avérous, 2015).

Our previous study shows TA can strongly retard the hydration of cement due to consumption of calcium ions during the formation of calcium chelate complex (Fang, 2021; Fang et al., 2021). Therefore, this study proposes a pre-hydration method to overcome this strong retarding effect of TA so that practical application of TA in concretes can be enabled. In this method, a small portion of OPC is first mixed with a TA solution with high-speed stirring. The presence of TA can significantly influence the hydration of cement. Particularly, spherical nanoparticles can be in-situ produced by this pre-hydration process due to the multiple interactions or reactions induced by TA. These in-situ produced nanoparticles can be well dispersed in the slurry due to the hydrophobic interaction generated by π-π stacking. This pre-hydrated slurry which has in-situ produced nanoparticles and TA is then mixed with other ingredients to produce the concrete. The nanoparticles produced in the pre-hydration process can serve as nucleation seeds for the growth of C–S–H, accelerating the hydration of the cement (Singh et al., 2013). Using in-situ produced nanoparticles in concrete can eliminate cost associated with filtering, drying, storage, and dispersing of the produced nanoparticles. In this way, the retarding effect of the TA can be significantly reduced and the benefits of TA on the performance of concrete discovered in our previous research (Fang, 2021; Fang et al., 2021) can be exploited without sacrificing the early age strength of the concrete.

The objective of this study is to evaluate the potential of the proposed pre-hydration method on the enhancement of the performance of cement mortars. To gain fundamental understanding on the underlying working mechanisms of the proposed pre-hydration method, a comprehensive experimental program was also carried out.

This study opens news routs and creates new opportunities to identify and design a new generation of chemical admixtures, which is renewable, low-cost, and nontoxic. Although extraordinary efforts have been made to reduce the global warming potential of concretes, most of these works focus on cements. Chemical admixtures, which are important parts of concretes, are predominately produced from fossil carbon source. The transition from this non-renewable source to renewable plant-carbon sources for admixture is necessary to achieve deeper reduction on the carbon emission associated with concretes.

2. Materials and methods

2.1. Materials

Type I Portland cement was used in this study to make all sample, which chemical composition is given by Table 1. Natural river sand with fineness modulus of 2.80 was used as aggregate purchased from Red Eagle Sand & Gravel in Alabama. Tannic acid ($C_{76}H_{52}O_{46}$, 98%) was purchased from Alfa Aesar.

2.2. Pre-hydration process via TA modification

The pre-hydration process was carried out through mixing a small amount of cement with the TA solution. The dose of TA added to the solution is a key factor of this pre-hydration process, which is given as the ratio between the TA and the total amount of cement used in the mortar mix (T/C). Five T/C ratios, namely, 0% (no TA), 0.1%, 0.3%, 0.5% and 1% were used to pre-hydrate the cement particles. In a typical pre-hydration process, the TA powder was dissolved in DI water under stirring for 5 min at the room temperature. The amount of water was the same amount of the mixing water needed for the mortar. Then 0.5% of the total cement used in the mortar mix was added into this TA solution under stirring at 700 rpm for 6h. After the pre-hydration process, extra deionized (DI) water was added into the slurry to compensate the loss of the mixing water during the pre-hydration process. The produced slurry was then directly used as the mixing water to produce mortar specimens.

2.3. Manufacturing and characterizing mortar specimens

2.3.1. Manufacturing process of mortar specimens

Four groups of mortar samples were manufactured with mix design shown in Table 2. In this table, PC and LPC were two control groups produced without using the pre-hydration process with water to binder (w/b) ratios of 0.55 and 0.45, respectively. Group PTX are cement mortars with a w/b ratio of 0.55 and made with pre-hydrating 0.5% cement in the mixing water with TA as 0.X% of the total cement in the mix. Mortar LTX are produced in the similar way as the PTX mortar, except that the w/b ratio is 0.45. All mortars were cast into 50 mm × 100 mm cylinder samples for compressive testing. The produced samples were moisture cured at 23 °C and relative humidity not less than 95%.

2.3.2. Characterizing the mortar specimens

(1) Compressive Strength

The compressive strengths of the produced mortar samples were measured by a Humboldt compressive strength testing machine with a 45 tons capacity. Three duplicated samples were tested at the ages of 3d, 7d, 28d, 90d, and 180d according to ASTM C39-18 (ASTM, 2018a). The loading rate was selected as 0.25 MPa/s. Capping pads were used to reduce the inaccuracy induced by the roughness of the cylindrical sample on the measured compressive strength.

(2) Isothermal calorimetry test

Isothermal calorimetry test was performed to evaluate the effect of the proposed method on the hydration kinetics of the cement by an I-Cal 4000 calorimeter at the ambient temperature of 23 ± 0.02 °C according to ASTM C1679-17 (ASTM, 2017). Testing samples were prepared by mixing 50 g cement with 25 g DI water or with the pre-hydrated cement slurry. The thermal power and accumulate heat energy of the reaction was recorded for the first 60 h. All the obtained values were normalized by the total weight of the cement (50g) in the sample.

(3) Spread flow and setting time

Table 1
Chemical composition of Type I Portland cement.

Composition	SiO_3	Al_2O_3	CaO	Fe_2O_3	TiO_2	MgO	Na_2O	K_2O	P_2O_5	LOI
(%)	22.93	4.68	64.04	2.41	0.20	3.38	0.23	0.76	0.08	0.82

Table 2
Mix design of the mortars produced by pre-hydration method.

Mortar	w/b	Water (kg/m^3)	Cement (kg/m^3)	Sand (kg/m^3)	Premixed Cement (kg/m^3)	TA content (wt. % of cement)
PC	0.55	264	480	1440	–	–
PT0	0.55	264	480	1440	2.4	–
PT1	0.55	264	480	1440	2.4	0.1
PT3	0.55	264	480	1440	2.4	0.3
PT5	0.55	264	480	1440	2.4	0.5
PT10	0.55	264	480	1440	2.4	1.0
LPC	0.45	216	480	1440	–	–
LPT0	0.45	216	480	1440	2.4	–
LPT1	0.45	216	480	1440	2.4	0.1
LPT3	0.45	216	480	1440	2.4	0.3
LPT5	0.45	216	480	1440	2.4	0.5
LPT10	0.45	216	480	1440	2.4	1.0

To estimate the consequence of the pre-hydration on the workability of the fresh mortar, the flow of the fresh mortar was tested at the room temperature of 23 ± 1 °C in compliance with ASTM C1437-15 (ASTM, 2015). The initial and final setting times of the cement paste were determined by the Vicat needle testing according to ASTM C191 (ASTM, 2008).

(4) FTIR and SEM analysis of the pre-hydration products

FTIR and SEM were carried out to examine the effect of the presence of TA on the hydration products of the cement. To this end, FTIR spectra of the solid powders filtered from the pre-hydrated cement slurry were obtained using a PerkinElmer Spectrum 2 with an attenuated total reflectance (ATR) accessory. The morphology of the nanoparticles was examined by a Field Emission SEM (JSM-7000F).

(5) X-ray powder diffraction (XRD)

XRD analysis was carried out to determine the mineral composition of the hydration products. To do this, the paste samples after calorimetry testing were cured in sealed conditions for 7d and 180d. Then these paste samples were crushed and ground into fine powders. #100 meshes (0.15 mm) were chosen to sieve the fine powders for XRD analysis. The analysis was carried out by using a Bruker D8 Discover with GADDS with the scan range 11.6–71.2°. Two separate frames were integrated for the final pattern. Each frame period run 180s with Co (40 kV, 35 mA) source and scan step 0.005°/s.

(6) Thermal gravimetric analysis (TGA)

TGA was used to quantify the hydration products of the cement. To this end, the samples prepared for XRD analysis will be also used for TGA using a PerkinElmer STA 8000 instrument. For each test, the sample was first held at 30 °C for 30 min, and then heated to 900 °C at 10.00 °C/min.

(7) Mercury intrusion porosimetry (MIP)

MIP was carried out to evaluate whether the proposed method can change the pore structure of the produced concrete. The crushed samples after the compressive strength test at the age of 28d were used in the MIP analysis with a Micromeritics AutoPore IV 9500.

(8) Grid Nanoindentation

Nanoindentation testing was carried out to reveal the micro-mechanical properties of the hardened cement pastes. The cement paste samples used in this testing have a water cement ratio 0.5 and were cured under sealing condition for 28 d. To this end, the freshly cut hardened cement paste section was cast into the capsule filled with epoxy resin, followed by being polished successively with SiC sanding paper and on felt cloth with 0.3 μm and 0.05 μm alumina suspensions (Fang, 2021; Tuinukuafe, 2019). A Histron TI950 nanoindenter was used to make 400 indents on a 20 × 20 grid with a 10 μm spacing. For each indent, the load was increased by multiple partial unloading (10 times) up to 1 mN, finally held for 2 s, and reduced linearly back to zero in 5 s (Chen et al., 2021). The Poisson ratio of the cement pastes was assumed as 0.2. Multiple cycles of partial loading and unloading were chosen to make each indent, thereby eliminating the creep, surface roughness and size effects (Mondal, 2008). The elastic modulus was calculated for each indent using the Oliver and Pharr method (Oliver and Pharr, 1992). The packing density of the hydration products at the location of each indent could be obtained based on the results of nanoindentation using Vandamme's method with a linear scaling relationship (Vandamme and Ulm, 2008, 2013), which is also described in detail in our previous studies (Fang, 2021; Fang et al., 2021).

For the heterogeneous and multiphase materials, it is essential to apply statistical deconvolution techniques to determine the volume fractions and the average mechanical properties of each phase. The deconvolution process was performed on MATLAB via Gauss Mixture Model (GMM) with the expectation maximization (EM) algorithm.

3. Results and discussion

3.1. Morphology of nanoparticles produced by pre-hydration with TA

At the end of the pre-hydration process, reaction products were filtered and examined by SEM and results are shown in Fig. 1. Plentiful hydration products such as ettringite, C–S–H, and calcium hydroxide (CH) could be easily identified in the control group (PT0), as shown in Fig. 1(a). The typical TA particle exhibits a porous structure beneath a smooth surface, as shown in Fig. 1(f). After pre-hydrating the cement in the TA solution, those typical shapes of the hydration products are not present. Instead, many spherical particles with a size in hundreds nanometer were produced and deposited on the surface of large particles, as shown in Fig. 1(b–e). These nanoparticles were formed by complexation between the calcium ions released from the cement and TA. It can be seen that large nanoparticles were produced with more TA in the solution. This is because more nanoparticles were induced by higher content of TA, which conglomerated more easily by the strong van der Waals forces during the drying procedure. It is of great significance to produce these nanoparticles in-situ, which are self-dispersed in the concrete. In this way, one of the significant barriers preventing the large-scale application of nanoparticles in concrete, dispersing nanoparticles, is eliminated. These small particles can function as nucleating seeds to facilitate the hydration of cement. Fig. 1(b–e) reveal that in-situ production of nanoparticles in concrete can be simply achieved by pre-hydrating a small amount of cement in the TA solution.

In addition to nanoparticles, a cracked shell can be observed for all powders produced by the pre-hydration with TA. This shell was produced by the deposition of the reaction products between the TA and the hydration products of cement, as revealed by the XRD and FTIR analysis shown in Figs. 2 and 3. This shell can slow down the further hydration of

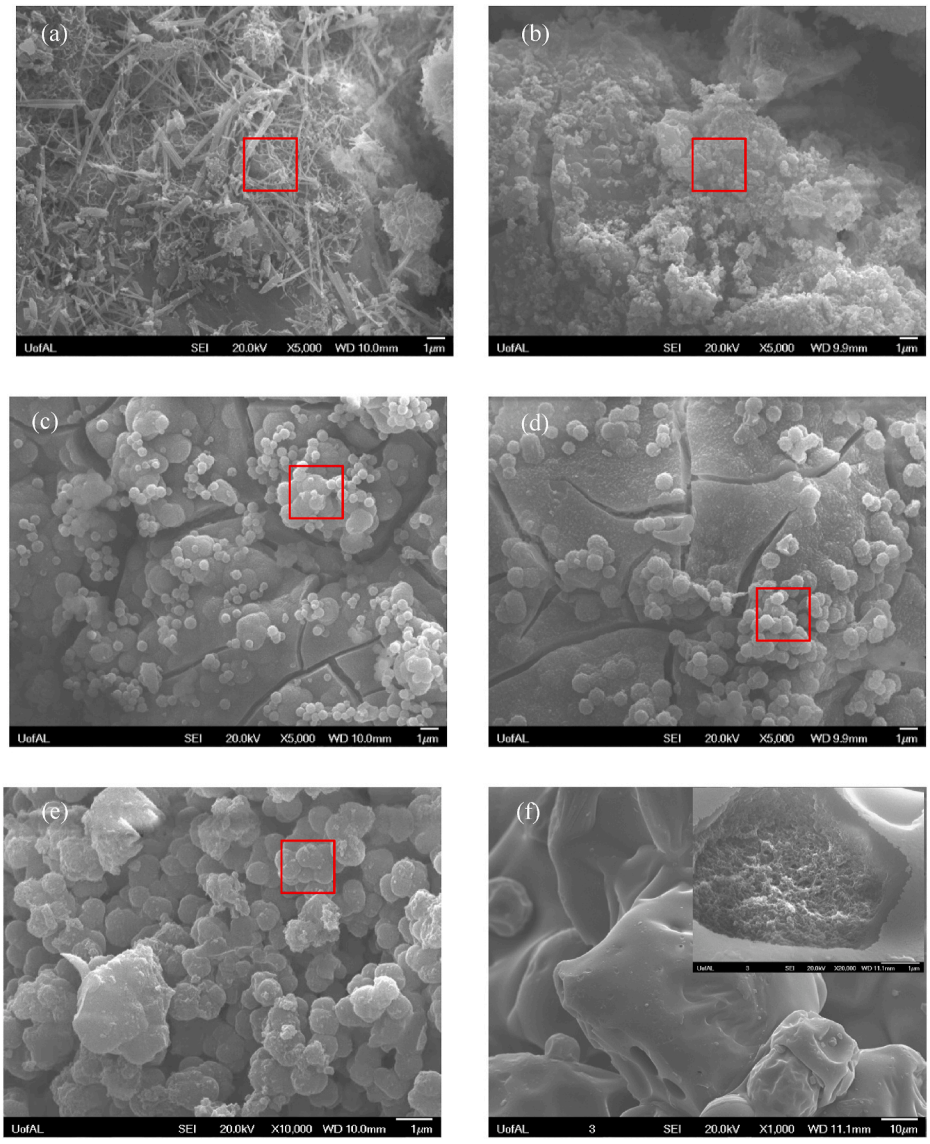

Fig. 1. SEM images of filtered particles produced by pre-hydration with TA: (a) PT0_Powder; (b) PT1_Powder; (c) PT3_Powder; (d) PT5_Powder; (e) PT10_Powder; (f) Pure TA powder.

the cement, leading to a significant retarding effect of the TA observed in the existing literature.

Table 3 summarizes the element distribution of the selected regions of the filtered particles after the pre-hydration process. Much more carbon elements were detected in the samples with TA, indicating TA was present in these nanoparticles. Both calcium and silica were reduced by the addition of TA, suggesting less C–S–H was produced and these nanoparticles are more likely calcium tannate, the complex between TA and calcium. Nevertheless, the carbon analysis in the EDS is not very reliable due to the contamination of CO_2 in the air, as well as the possible interference of the carbon tape fixed with the aluminate holder. Further investigation is needed to determine the detailed chemical composition and structure of the pre-hydration products.

3.2. XRD and FTIR results of the minerals produced by pre-hydration with TA

Hydration products produced by the proposed pre-hydration process were further characterized by XRD and FITR. To this end, ethanol was immediately added into the pre-hydrated cement slurry to stop the hydration of the cement. Then the reaction products and unreacted cement particles were filtered and dried under vacuum for 48h and then pulverized into powder passing through #100 sieve. These powder samples were noted as "PTX_Powder", indicating that they were produced by pre-hydrating 0.5% cement in the solution with TA added at T/C of X ‰ (X/1000). These powder samples were then examined by XRD and FTIR.

XRD patterns of these powders are shown in Fig. 2. In addition to the alite (C_3S) in the anhydrate cement, hydration products of cement such as CH and ettringite, and calcite ($CaCO_3$) are also present in these powders. The presence of calcium carbonate is anticipated since CH can be quickly carbonated in the air. No C–S–H is detected in the powder since it is amorphous and very little was produced by the pre-hydration process. With more TA used in the pre-hydration solution, the intensities of CH, calcite, and alite peaks all are reduced. Reduction of the intensities of CH and calcite peaks is expected since more CH and calcite can be consumed by adding more TA through the reaction between the TA and CH and calcite. The products of the reaction, together with other amorphous hydration products and TA were deposited on the surface of the filtered powders, leading to the reduction of the intensities of all three minerals. Indeed, a broad hump between 20° and 40° appears on the XRD curves of PT_5 and PT_10 samples, confirming that the amorphous material was produced in these samples. This amorphous material

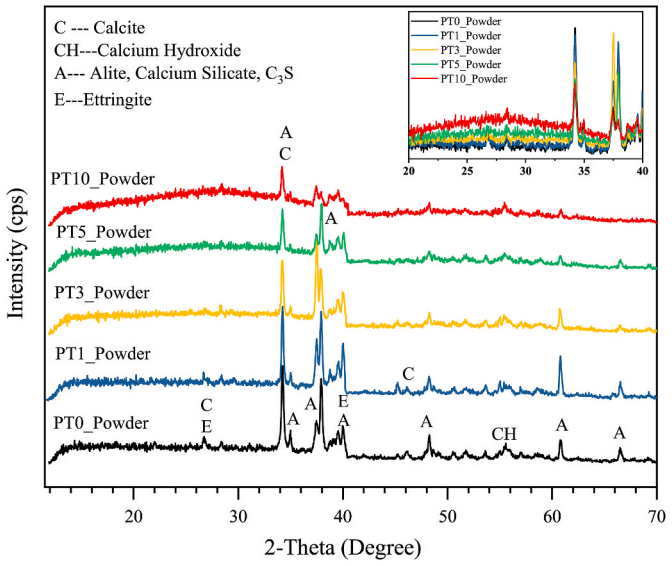

Fig. 2. XRD patterns of produced filtered powders after the pre-hydration process.

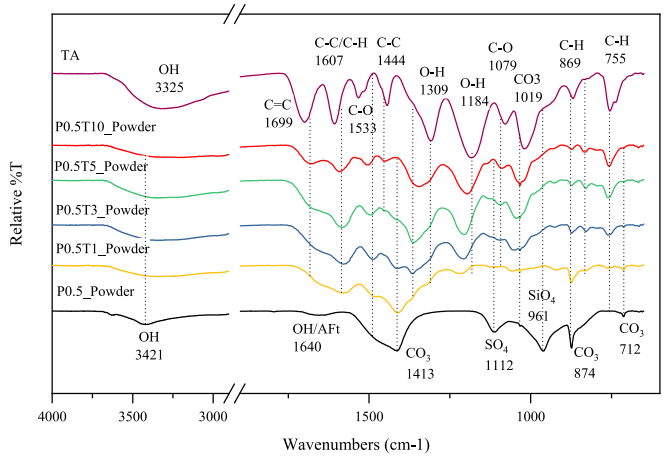

Fig. 3. FTIR patterns of produced filtered powders by the pre-hydration process.

Table 3
Element distribution of the filtered particles obtained from EDS analysis from the red region in Fig. 1.

Element	Ca (wt.%)	C (wt.%)	O (wt.%)	Si (wt.%)	Al (wt.%)
PT0	42.3	6.5	38.7	9.4	3.1
PT1	44.1	18.3	27.6	7.0	–
PT3	21.8	37.6	33.6	3.8	–
PT5	18.2	39.1	38.1	3.9	–
PT10	13.5	46.7	36.1	2.9	–

is most likely the complex of calcium and TA, which was then examined by FTIR.

Fig. 3 shows the FTIR patterns of the filtered powders, and Table 4 presents the assignments of spectral peaks. For the control group PT0, the broadband in the range of 3550–3100 cm^{-1} is the characteristics of –OH stretching for the hydrogen bond with physically adsorbed water molecules. A peak at 1640 cm^{-1} is due to the bending vibration ν_2 of water in sulfates (Hughes et al., 1995; Ren et al., 2014). The peaks at 1413, 874, and 712 cm^{-1} can be attributed to the carbonation of the CH in the air, or the calcium carbonate that was present in the cement as

Table 4
FTIR properties of TA, and filtered powder by using the pre-hydration process with or without TA (wavenumber: cm^{-1}) (Wang et al., 2020).

TA	PT0	PT1	PT3	PT5	PT10	Assignment
3325	3421	3339	3329	3344	3210	(-OH) stretch in H_2O
1699	–	–	–	1679	1680	(C═C) stretch of benzene ring
–	1640	–	–	–	–	(O–H) bending vibration ν_2 of in sulfates
1607	–	1579	1579	1583	1592	(C–C) stretch and (C–H) deformation in plane of benzene ring
1533	–	1485	1489	1495	1502	(C–C) stretch and (C–H) deformation in the plane of benzene ring, (C–O) stretch of phenolic
1444	–	–	–	–	–	(C–C) stretch of benzene ring and methylene, and (C–O) stretch of phenolic
–	1413	1411	1412	–	–	(C–O) stretch and out of plane bending
1309	–	–	1365	1363	1346	(C–O) stretch and (O–H) deformation of phenolic, (C–C) stretch and (C–H) deformation in the plane of benzene ring
1184	–	1216	1209	1206	1196	(O–H) deformation in the plane of phenolic and carboxylic acid, (C–C) stretch and (C–H) deformation in the plane of benzene ring
–	1112	–	–	–	–	($SO4^{2-}$) bending vibration ν_3 in sulfates
1079	–	–	1095	1095	1090	(C–O) stretch of phenolic, ether and carboxylic acid
1019	–	1057	1051	1045	1033	(C–O) stretch of ether and carboxylic acid
–	961	–	–	–	–	($SiO4^{2-}$) out of plane bending vibrations
–	874	873	873	873	873	(O–C–O) split in the plane of bending vibrations
869	–	–	–	–	–	(C–H) deformation out of plane of benzene ring
755	–	762	759	759	757	(C–H) torsion of benzene ring
–	712	713	712	–	–	(O–C–O) out of plane bending vibrations

Note: To shorten the length of the name of the samples, "_Powder" is omitted for this table. Besides, the symbol "-" means the data are not available in the figure.

fillers (Delgado et al., 1996). A characteristic sulfate absorption band is generally seen in the range 1100–1200 cm^{-1} due to the ν_3 vibration of the SO_4^{2-} group in sulfates. The absorption band at 961 cm^{-1} belongs to C–S–H. The absorption spectrum at 874 cm^{-1}, which deepens with time, is induced by the dissolution of the C_3S (Björnström et al., 2004).

The characteristic peaks in the TA are as follows: the stretch of (C = C) of the benzene ring band at 1699 cm^{-1}; the stretch vibration of (C–C) of the benzene ring band at 1607, 1533, 1444, 1309 cm^{-1}; the deformation in-plane (C–H) of the benzene ring band at 1607, 1533, 1309, and 1184 cm^{-1}; the deformation out of the plane (C–H) for the benzene ring band at 869 cm^{-1}; the stretch (C–O) of the phenolic band at 1533, 1444, 1309, and 1079 cm^{-1}; the stretch (C–O) of the carboxylic acid and ether band at 1079 and 1019 cm^{-1}; the deformation (O–H) of phenolic at 1309 and 1184 cm^{-1}; and finally the torsion vibration (C–H) of the benzene ring at 755 cm^{-1} (Çakar and Özacar, 2016).

Comparing the spectrum of powder produced by pre-hydration in TA solution (PTA) with that of the control group (PT0) shows the peaks of carbonate (C–O) deformation with 1413, 874, and 712 cm^{-1} are weakened gradually with the increase of TA concentration. This can be attributed to the neutralization reaction between the CH and the TA which consumes CH, or the retarding effect of the TA which produces less CH. In addition, the peaks of C–S–H located at 961 cm^{-1} and the SO_4^{2-} group in sulfates located at 1112 cm^{-1} disappear due to the addition of the TA. This indicates that the reaction products covered the

surface of the cement particles as shown in Fig. 1 or that calcium ions were consumed by the reaction with TA. For a similar reason, the peak of the O–H in the water of the sulfates disappears. Of course, the overlap of the peak of (C═C) at 1699 cm^{-1} with the peak of O–H may overshadow this peak.

Comparing the spectrum of the PTA with that of the TA shows that the peaks at 1699, 1607, 1533 cm^{-1} are redshifted, and the peaks at 1309, 1184, 1079, 1019, 755 cm^{-1} are blue-shifted with the reduction of the concentration of the TA. The reduction of the wavenumber in redshift is caused by the hydrolysis of the TA in the alkali environment created by the hydration of the cement (Iibuchi et al., 1972). The increase of the wavenumber for the blue-shift can be attributed to the neutralization reaction between the TA and the CH, the complexation reaction, and chelation reaction of TA with metal ions such as Ca^{2+}, Fe^{3+}, Al^{3+} (Kim and Pasc, 2017). All these suggest the presence of strong interaction between Ca^{2+} and TA. Therefore, TA-Ca complex can be formed during the hydration of the cement due to the coordination of phenolic-OH group with calcium ions through deprotonation.

3.3. Effects of pre-hydration in TA solution on the properties of mortars

3.3.1. Flowability, setting time and heat evolution

Fig. 4(a) presents the flowability of fresh mortars produced by the proposed pre-hydration process. Simply pre-hydrating 0.5% cement in the mixing water (PT0) reduced the workability of the mortars by 3%, in comparison with the plain group (PC). This is expected since the hydration products in the pre-hydration slurry without TA such as CH, C–S–H, and ettringite can function as nuclei for new hydration products. As a result, the early age hydration of the cement was accelerated by the pre-hydration cement slurry without adding TA, leading to a lower flowability of this group of fresh mortar. After pre-hydrating the cement in the TA solution at T/C = 0.1%, the workability of the mortar was recovered to the same as that of the plain group (PC), suggesting that TA can be used to disperse cement particles. This dispersion function of TA can be attributed to the steric repulsion between individual minerals induced by the TA (Lin and Xing, 2008). For this reason, the workability of the mortar increases with the content of TA used in the pre-hydration process, as revealed by Fig. 4(a).

Fig. 4(b) shows the effect of pre-hydration on the set times of the produced pastes. Compared to the PC group, both the initial and final set times of the pastes produced with the pre-hydration without TA (PT0) were slightly reduced. This agrees with the observation on flowability shown in Fig. 4(a), confirming that pre-hydrating a small amount of cement in pure water can slightly accelerate the hydration of the cement. When mixing the paste by pure TA solution with T/C = 0.3% (T3), the initial and final set times were significantly delayed by 138 and 368 min, respectively, compared to that of the plain group PC. The retarding effect of TA has been found for over 100 years (Abrams, 1920). As demonstrated by existing studies, organic molecules or polymers can be adsorbed on the un-hydrated cement particles, preventing the attack by water, and thus retarding the hydration of the cement (Hansen, 1960). Compared with these organic molecules and polymers, TA has an even stronger capability to adhered to cement particles through covalent and noncovalent interactions, leading to severe retarding of the hydration of the cement.

The pre-hydration method is proposed to mitigate the strong retarding effect of TA, which can be confirmed by Fig. 4(b). The initial and final set times of the mortar (PT3) were reduced by 100 and 305 min, respectively, after pre-hydrating 0.5% cement in the 0.3% TA solution (T3). This can be attributed to two effects induced by the pre-hydration process: less free TA is available to retard the hydration of the cement and many nanoparticles are in-situ produced in the fresh concrete, which seed the hydration of the cement (Singh et al., 2013).

It is observed that the set times of the mortars increase with the content of TA used in the pre-hydration. This is expected since more free TA molecules are available to retard the hydration of the cement in the mortar with a higher concentrated TA solution. Nevertheless, set times for all samples except PT10 are no more than 90 min longer than the control one, meeting the requirement of ASTM C191 (ASTM, 2018b). PT10 exhibits a slightly shorter initial set time than the PT5 sample even though much more TA was added. This can be attributed to the reaction between TA and some cement hydration products. As shown in Fig. 1, the products of this reaction were deposited on the surface of the unreacted particles to form a shell. If sufficient such products are produced in the fresh mortar due to the higher content of TA, the mortar can lose its plasticity, and the initial set starts.

The effect of the proposed pre-hydration process on the hydration of the cement paste can be revealed by the calorimetry test results shown in Fig. 5. Compared with the plain group PC, pre-hydrating 0.5% cement in water slightly reduces the dormant period of the cement, but significantly reduces the peak of the thermal power of the hydration of cement, as revealed by the PT0 curve in Fig. 5(a). Consequently, less accumulated heat is produced by the hydration of the PT0 sample than that generated by the hydration of the PC within the observing period, suggesting that pre-hydration without TA suppresses the hydration of the cement at an early age. In addition, many ions such as Ca^{2+} are produced in the mixing water by the pre-hydration, which can reduce the time needed for these ions to reach saturation in the fresh mortar. As a result, the dormant period for PT0 was slightly reduced and more precipitate were produced at the early stage. The precipitants covered the surface of the cement particle, leading to lower peak power heat observed in Fig. 5 for PT0.

Retarding effect of TA could be seen in Fig. 5. The heat flow peak corresponding to the hydration of C_3S was delayed by around 30h in T3, agreeing very well with the measured setting time shown in Fig. 4(b). As a result, the total heat was reduced to 54% by 60h. As mentioned before, the retarding effect can be attributed to the formation of calcium chelate complex and the absorption on the un-hydrated cement particles. The former causes the consumption of calcium ions, while the later prevents the attach by water. The retarding effect can be effectively mitigated by

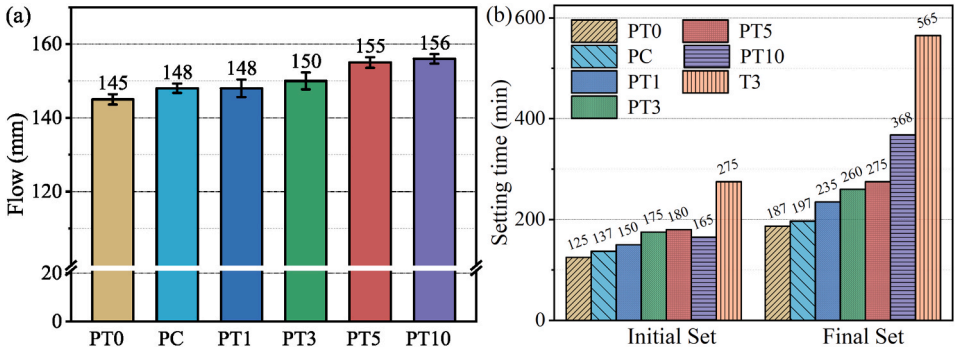

Fig. 4. Properties of the fresh mortars mixed with pre-hydration process: (a) flowability (mm) and (b) setting time.

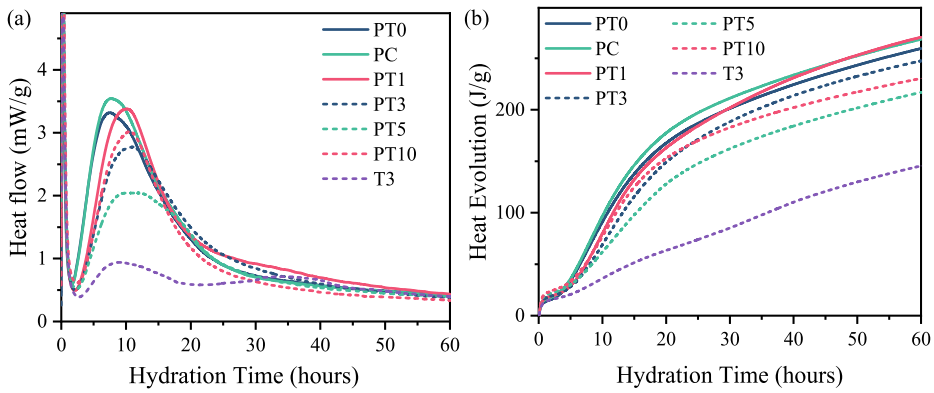

Fig. 5. Effect of the proposed pre-hydration process on the hydration of the cement: (a) thermal power; (b) Accumulated hydration heat.

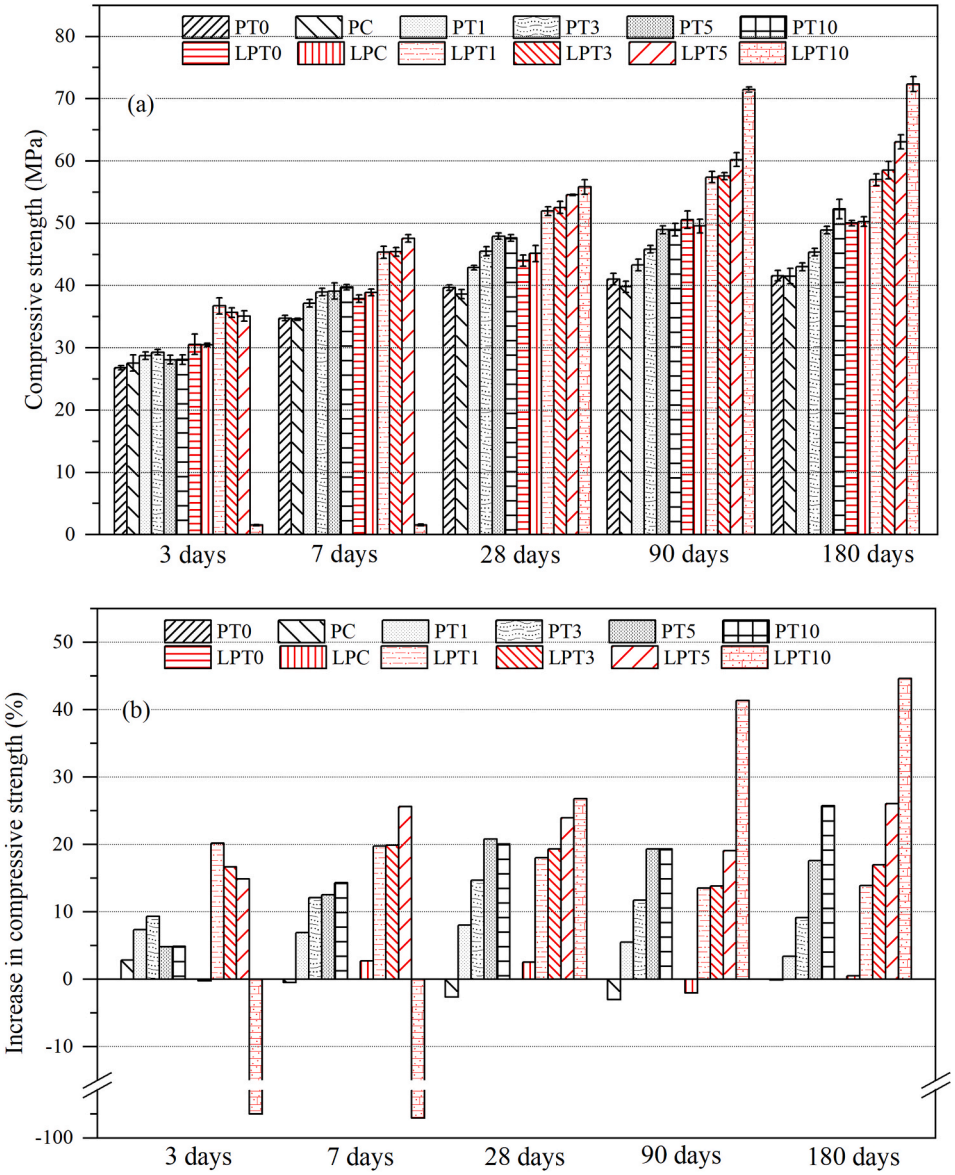

Fig. 6. Improvement on the compressive strengths achieved by the proposed method: (a) the compressive strength; (b) the increase % compared to the compressive strength of the control groups PT0 or LPT0.

pre-hydrating 0.5% cement in the TA solution. As revealed by the curve PT3 in Fig. 5(a), the peaks of hydration are shifted left to just 3.5h later than that of the control sample (PC). Consequently, the total heat generated by the hydration is significantly improved (Fig. 5(b)). This is because the TA modification not only reduces the free TA molecules in the solution but also promotes the hydration of cement due to filler effect and nucleation effect of produced nanoparticles.

The retarding effect of the TA can be further reduced if less TA is used as revealed by the heat flow of the PT1 sample in Fig. 5(a). It has a peak even higher than that of PT0. Although the peak of the heat power of this sample is lower than that of the PC, its total heat is higher at the end of the observation, indicating that pre-hydration in the TA solution facilitates the hydration of PT1 group. This is not surprising since the in situ produced nanoparticles via TA modification can serve as nucleation sites for the growth of C–S–H, promoting the hydration of cement. Of course, when more TA was used in the pre-hydration process, a more severe retarding effect can be observed, as shown by PT5 and PT10 samples since more free TA is available in the samples. Moreover, the hydration kinetic results indicate the proposed method modified the exothermic process of cement hydration and mitigates the cumulative heat, which might provide another effective solution of the thermal cracking issues (Yan et al., 2020, 2021).

3.3.2. Compressive strength of the mortars

Fig. 6 presents the compressive strength of the produced mortars at 3d, 7d, 28d, 90d, and 180d. For the mortars with w/c = 0.55, the compressive strength of the control group (PT0) is 2.84% lower than the plain group (PC) at 3d but surpasses that of the PC at 7d, 28d, 90d, and 180d by 0.48%, 2.63%, 3.01%, and 0.12%, respectively. This agrees with the calorimetry testing result shown in Fig. 5, which indicates that hydration heat produced by the PT0 is lower than that of the PC at first 30h but surpasses that of PC after that. After pre-hydrating the cement with TA solutions, much more improvement on the compressive strengths can be achieved for mortars at all ages. The compressive strengths of PT3 at 3d, 7d, 28d, 90d, and 180d exceed those of the PC by 9.33%, 12.14%, 14.70%, 11.74%, and 9.18%, respectively. If 0.5% TA is added, the compressive strengths of the mortar (PT5) at 3d, 7d, 28d, 90d and 180d are improved by 4.93%; 12.54%, 20.85%, 19.32% and 17.62%, respectively. Compared with PT3, PT5 has a slightly lower strength at 3d due to stronger retarding effect induced by more free TA in the mix. However, the compressive strength of PT5 was higher after 3d, suggesting that stronger concrete can be produced by adding more TA. This can be confirmed by the compressive strength of PT10, which surpasses that of the PC by 4.91%, 14.34%, 20.11%, 19.32% and 25.76% at age of 3d, 7d, 28d, 90d, and 180d, respectively. The significantly strength enhancement is attributed to the filler and nucleation effects of the in-situ produced nanoparticles, as well as the dispersing effect and microstructure refinement of TA (Fang et al., 2021).

A similar trend could be observed for the mortars with a lower w/c (0.45). As shown in Fig. 6, the compressive strength of LPT0 is close to that of the plain group (LPC) within acceptable experimental error. With the pre-hydration process in TA solution, the compressive strengths have been significantly enhanced for all ages, except the group LPT10. Similar to the previous case, higher strength improvement has been achieved by using more TA in the pre-hydration process. Overall best strength improvement was reached by LPT5 mortar, which exhibits a compressive strength improvement over the control group (LPC) at 3d, 7d, 28d, 90d, and 180d by 14.90%, 25.62%, 23.96%, 19.08%, and 26.05%, respectively. However, when TA is added at T/C = 1%, the retarding effect of the TA becomes too strong to be mitigated by the proposed pre-hydration method, as indicated by low compressive strengths at 3d and 7d. Compared with PT10, LP10 has more cement and less mixing water, leading to higher concentration of free TA molecules in the pre-hydrated slurry. This suggests that the retarding effect is mainly determined by the concentration of TA in the solution, not total amount of TA added to the mortar. Nevertheless, LPT10 recovered its compressive strength rapidly after 7d, drastically surpassing those of the control sample at later age. It can be seen that better strength improvement can be achieved by the proposed method for the cement mortar with lower w/c ratio. This improvement can significantly increase the eco-efficiency of cement, which will be discussed in the later section.

3.3.3. Hydration products

Fig. 7 shows the XRD patterns of the produced pastes after sealed curing for 7d and 180d. Major crystalline minerals found in the pastes include typical hydration products such as CH and ettringite, alite from un-hydrated cement particles, and calcite induced by the carbonation of the CH in air. Since most of the C–S–H is amorphous, it cannot be detected from the XRD patterns shown in Fig. 7. At 7d, the intensities of the peaks of CH in the experimental groups (PT1, PT3, PT5, and PT10) were lower than that of the control group PT0. This can be attributed to either the retarding effect of TA on the hydration of the cement to produce less CH or the reaction between TA and CH to consume some produced CH. In particular, the peak of alite (37.90°) in PT10 was much higher than that of the control group PT0, suggesting that retarding effect of TA in this mortar was very high and much more un-hydrated

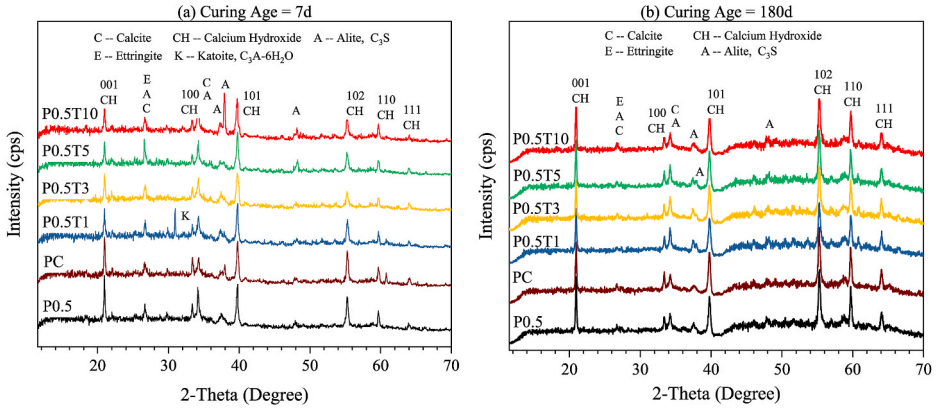

Fig. 7. XRD patterns of produced pastes after sealed curing for (a) 7d; (b) 180d.

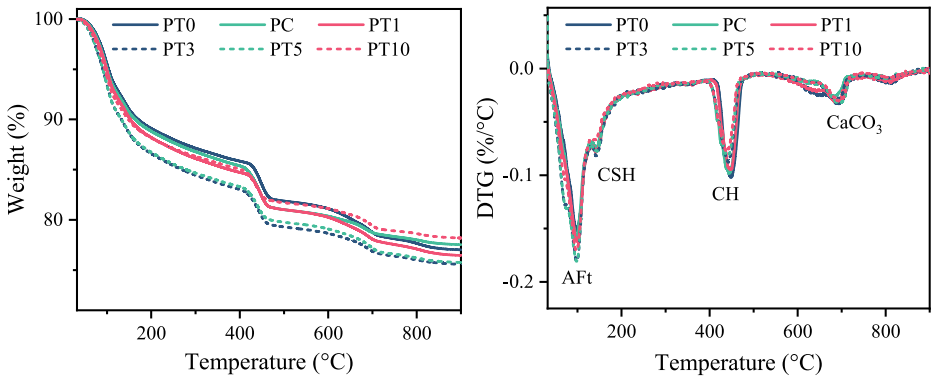

Fig. 8. TGA curves of the produced pastes after 7d sealed curing with the pre-hydration process.

cement is present in this mortar at this age. After curing for 180d, no distinctive difference could be found between the XRD patterns of all groups, as shown in Fig. 7(b). This is because the retarding effect of TA has diminished over 180d, which is consistent with the results from other organic retarders (Knapen and Van Gemert, 2009).

Since the quantitative analysis of the hydration product based on these XRD is not accurate, TGA was then carried out to examine whether the pre-hydration method can affect the hydration products of the cement at the early age. Fig. 8 presents the TGA results of the pastes produced for calorimetry test after 7d sealed curing. Existing studies suggest that typical decomposition temperature intervals for the hydration products of cement AFt, C–S–H, CH, and calcite are 80–130 °C, 120–160 °C, 400–500 °C, and 600–800 °C, respectively (Park et al., 2016; Rupasinghe et al., 2017). Corresponding to the decomposition of these four minerals, four main peaks appear on the derivative weight loss (DTG) curves of all samples, as labeled in Fig. 8. Loss of bound water from the C–S–H starts at 105 °C and mainly occurs at 120–160 °C, which partially overlaps with the decomposition temperature of ettringite. This makes it difficult to estimate the exact weight loss of ettringite. Nevertheless, the weight loss between 80 °C and 105 °C can be considered mainly due to the decomposition of ettringite (Qian et al., 2018).

Table 5 shows the calculated weight losses of AFt, C–S–H, CH, and calcite based on the temperature intervals mentioned above. The weight loss between 30 °C and 900 °C is a measure of bound water during hydration and, therefore, of the degree of hydration (Knapen and Van Gemert, 2009), as also shown in Table 5. Since the samples were cured in the open air, some of CH was carbonated. Therefore, the total CH content shown in the last column of this table includes both the CH calculated based on loss of the water in the peak of calcium hydrate (400–500 °C) and the equivalent molecular weight of CH based on the loss of CO_2 in the peak of calcite (600–800 °C).

Table 5 shows that both the total amount of CH and the bond water of control group PT0 are higher than those of the plain group PC. This is because extra 0.5% of cement was used in the pre-hydration. All mortars except PT10 produced by the pre-hydration with TA possess more bound water or higher degree of hydration than the PT10, suggesting that hydration of the cement was promoted by TA after 7d. Similar trend can be observed for the amount of C–S–H. All these agree well with the results of the compressive strength testing shown in Fig. 6. However, the change in the amount of total CH is not in accord with that of the bound water. For all the experimental groups, the amount of CH decreases with the increase of TA used in the pre-hydration. This is because: (1) TA can react with CH to reduce the amount of CH; (2) TA can retard the hydration of the cement to produce less CH.

Table 5
Calculated weight loss and bound water based TGA results of the produced mortars.

Temp. (°C)	Weight loss (%) related to the decomposition of					
	Ettringite 80-105	C–S–H 120-160	CH 400-500	Calcite 600-800	CH Total (%)	Bound water (%)
PT0	3.29	2.77	3.98	3.45	22.14	22.99
PC	3.50	2.67	4.37	2.38	21.95	22.47
PT1	3.55	2.82	3.71	3.16	20.57	23.54
PT3	3.98	2.89	3.75	2.63	19.83	24.42
PT5	4.03	2.86	3.55	2.89	19.44	24.24
PT10	3.74	2.48	3.33	2.50	17.90	21.80

3.4. Porosity and pore size distribution of the mortars

Porosities of the produced mortars produced by the pre-hydration process obtained by MIP are presented in Table 6. It shows that the proposed pre-hydrating method can reduce the porosity of the mortars. The total porosities of the mortars are reduced from 16.06% of PT0 to 12.53%, 13.93%, and 13.25% by adding 0.3%, 0.5% and 1% TA, respectively. Such a high reduction in porosity can lead to the much higher compressive strength of the mortar, as shown in Fig. 6.

The pore size distributions of the control group (PT0) and three experimental groups (PT3, PT5, PT10) are presented in Fig. 9. All the mortars have a similar distribution for pores with sizes larger than 10 μm. There is a significant sharp peak around 2 μm for the group PT5. The occasional entrapped voids and damage induced during the sample preparation might cause this abnormal peak. Nevertheless, the rest pre-hydrated groups show a similar distribution of pore sizes as the control group. The most significant difference between the mortar pre-hydrated without TA and those with TA appears on capillary pores with size between 10 nm–50 nm. Pre-hydration with TA significantly reduces these micro capillary pores, especially those meso gel pores smaller than 30 nm, as indicated by Fig. 9. This can be attributed to the nucleation and

Table 6
Porosity for pre-hydration mortar with TA obtained from MIP.

Specimens	PT0	PT3	PT5	PT10
Porosity (%)	16.06	12.53	13.93	13.25

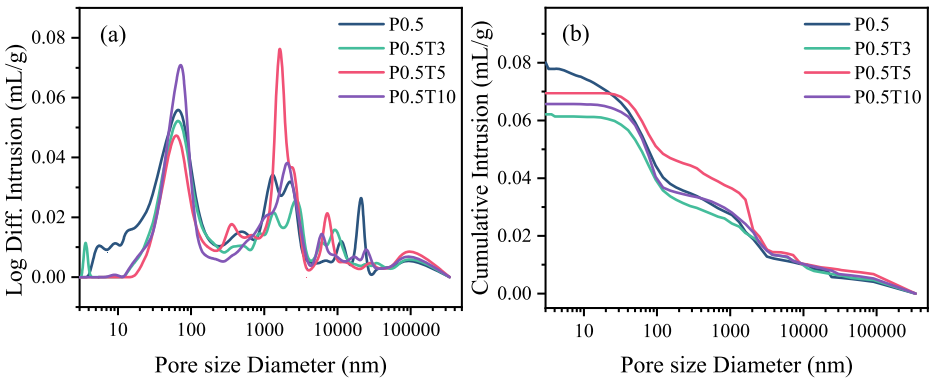

Fig. 9. Pore size distribution for the mortars mixed with prehydration process: (a) Log differential intrusion; (b) Cumulative intrusion.

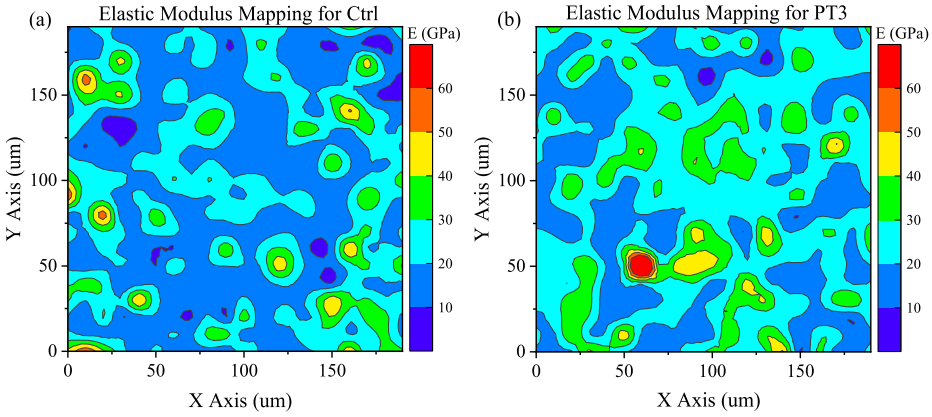

Fig. 10. Contour mapping of elastic modulus obtained from grid of nanoindentation: (a) Control cement pastes (Ctrl); and (b) Cement paste made by premixing with 0.3% TA (PT3).

filler effects of the produced nanoparticles, as well as the strong interaction between TA and the hydration products. This interaction can compact the hydration products into denser precipitate, leading to much lower capillary pore content and higher packing density (Fang et al., 2021). Although pores in this region do not strongly affect the strength of the mortar, they play essential roles in the long-term durability of the mortar because both the drying shrinkage and creep of concrete are determined by these pores.

3.5. Grid nanoindentation

Fig. 10 compares the contour mapping of elastic modulus obtained from grid nanoindentation tests for the control group and the cement pastes made with the pre-hydration process (PT3). The indents on C–S–H phases were recognized by the elastic modulus lower than those of the anhydrate cement particle (E > 60 GPa) (Pellenq et al., 2009). In the indent area, the cement pastes made with pre-hydration with 0.3% TA has higher elastic modulus than the one made without TA. This indicates that a dense microstructure was produced in the hydration products due to the pre-hydration with TA. A higher elastic modulus in the cement paste also suggests that better bonding between the hydration products can be achieved by the pre-hydration process, which also contributes to the higher compressive strength of the mortar, as shown in Fig. 6.

In grid nanoindentation testing, four phases of the hydration products (excluding anhydrous clinker minerals) can be identified based on the deconvolution results, which are porous phases (PP), low density C–S–H (LD), high density C–S–H (HD), and ultra-high density (UHD) C–S–H (which is essentially a mix of C–S–H with portlandite (Tennis and Jennings, 2000)), in the order of the lowest to the highest elastic modulus. Both LD and HD C–S–H are made of the same, almost compact (11% porosity), nanosized building blocks (4–5 nm). Nevertheless, they differ by their aggregation densities.

Figs. 11 and 12 present the deconvolution results of the elastic modulus and packing density obtained from the nanoindentation testing for the control group and PT3. In these figures, π is the volume fraction of the phase, μ is the mean value (in GPa) and σ is the standard deviation (in GPa). The volume fractions obtained from the deconvolution of the elastic modulus and the packing density show slight difference for both samples. However, the mean values of the elastic moduli for PP, LD, and HD phases are enhanced by 3.63, 3.57, and 5.77 GPa, respectively, by the pre-hydration of cement with 0.3% TA. Similar trend can be observed on the mean values of the packing densities, which are increased by about 0.03 for PP, LD, and HD phases due to the pre-hydration process. The only exception is the UHD phase, which has a lower modulus and a lower packing density after pre-hydration with TA. This reduction is likely induced by the complexing of Ca^{2+} ions by TA in CH, forming precipitate softer than the CH crystal. Overall, the total

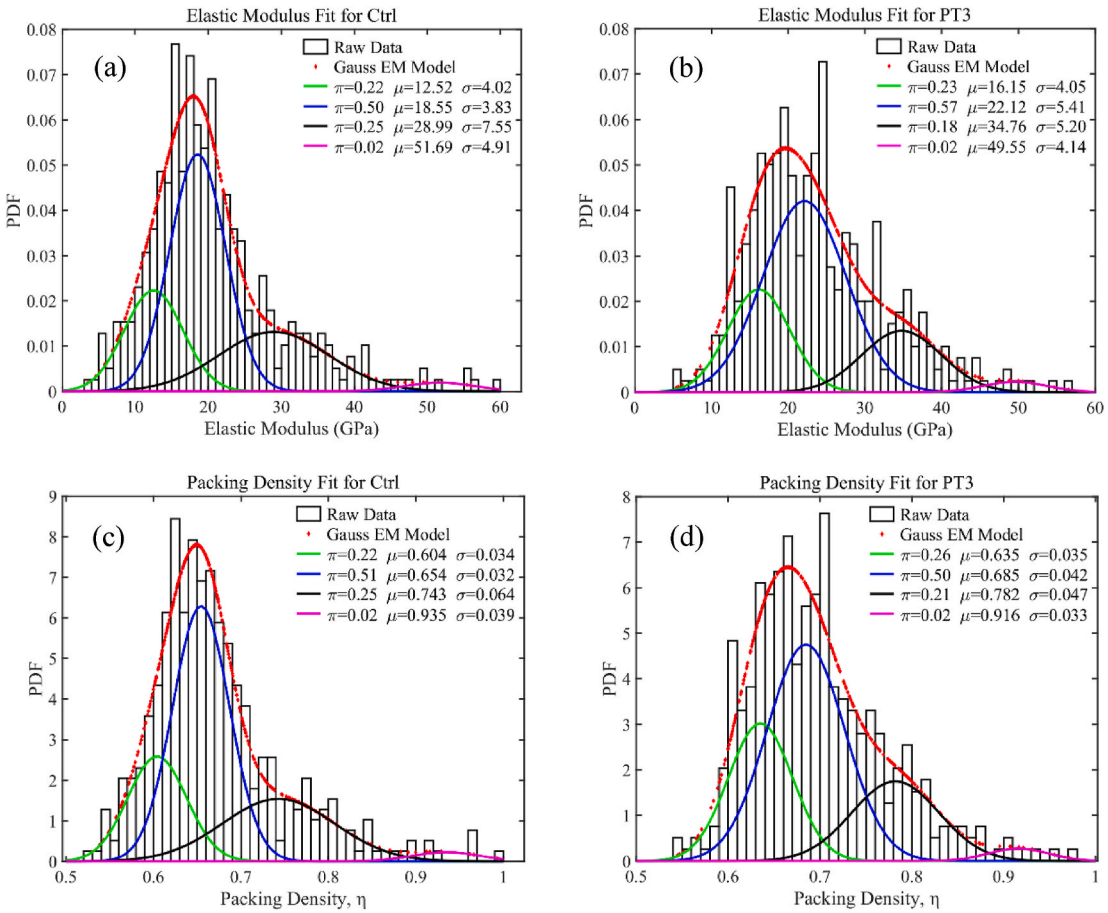

Fig. 11. Deconvolution results of the elastic modulus (E) and packing density (η) of nanoindentation: (a) The elastic modulus for Ctrl; (b) The elastic modulus for PT3; (c) The packing density for Ctrl; and (d) the packing density for PT3.

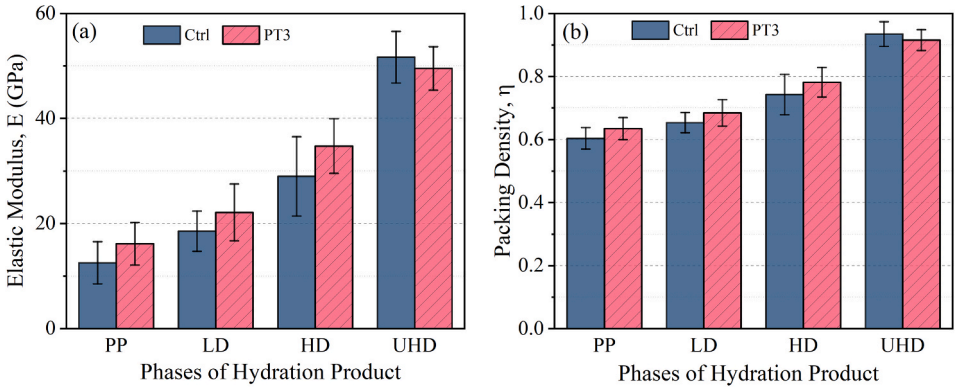

Fig. 12. Comparison of indentation properties of four different phases of hydrates for Ctrl and PT3: (a) Elastic modulus; and (b) Packing density.

elastic modulus and packing density of the C–S–H gels in PT3 were improved by 16% (from 20.31 GPa to 23.57 GPa) and 3% (from 0.670 to 0.690), respectively.

The higher packing density induced by TA can be attributed to the filler effect of the produced nanoparticles and the strong ability of the residual TA to bind to the hydration products. This binding ability of the TA molecules logically compact the loosely packed hydration products into a denser structure. This compacting ability of TA is so strong that it can completely change the morphology of the hydration products at early ages as revealed by Fig. 1. This also agrees well with the finding obtained from MIP results shown in Fig. 9, which revealed that nano-scale capillary pores were significantly reduced by the compacting ability of TA. With more densely packed hydration products, the compressive strength of the mortar is therefore enhanced, as shown in Fig. 6.

3.6. Economical and environmental analysis

The estimated embodied carbon and the costs of raw material of produced mortars are presented in Table 7 according to previous studies. TA is mainly derived from renewable plants, and can be extracted from industrial waste and byproducts, and therefore, has a lower carbon footprint (San Michele Mondovì and Gotti, 2016) in comparison with petroleum based admixtures.

Table 7
Embodied carbon and material costs of raw materials.

Materials	Embodied carbon (metric ton eq. CO_2/ metric ton)	Material costs (USD/ metric ton)
Cement	0.82 (Flower and Sanjayan, 2007)	124
Sand	0.0139 (Turner and Collins, 2013)	10
Water	0.001 (Yu et al., 2020)	0.5
TA	2 (San Michele Mondovì and Gotti, 2016)	1000

The environmental impact assessment can also be evaluated by the eco-strength efficiency of the mortars. The eco-strength efficiency can be regarded as the inverse of CO_2 intensity indicator, which is defined as the amount of CO_2 emitted to deliver one unit of performance (Damineli et al., 2010):

$$Eco-efficiency = \frac{Compressive\ strength\ at\ 180d}{Embodied\ carbon} \quad (1)$$

The cost-benefit of the concrete is a vital factor for the construction industry. The cost benefit can be defined as the amount of performance, i.e., compressive strength at 180d, for one unit of cost (per dollars):

$$Cost-benefit = \frac{Compressive\ strength\ at\ 180d}{Total\ material\ prices} \quad (2)$$

Based on the mix proportions of mortars, the embodied carbon, the eco-efficiency, the material costs, and the cost-benefit of mortars with w/b of 0.45 are estimated and summarized in Fig. 13. The proposed prehydration method generate little extra carbon emission due to near zero carbon footprint of TA and low dosage of extra cement (0.5%). Besides, it has slight influence on the materials cost due to the cheap raw material (cement and TA) and low dosage of TA (<1%). However, due to the significantly strength enhancement achieved by the dilute cement slurry modified by TA, the eco-efficiency and cost-benefit increases significantly over the content of TA. This indicates the TA modification has better sustainability and higher cost efficiency. As a result, LPT10 has the best overall performance due to the cumulative benefits: good mechanical properties, low carbon footprint, and high efficiency for sustainability.

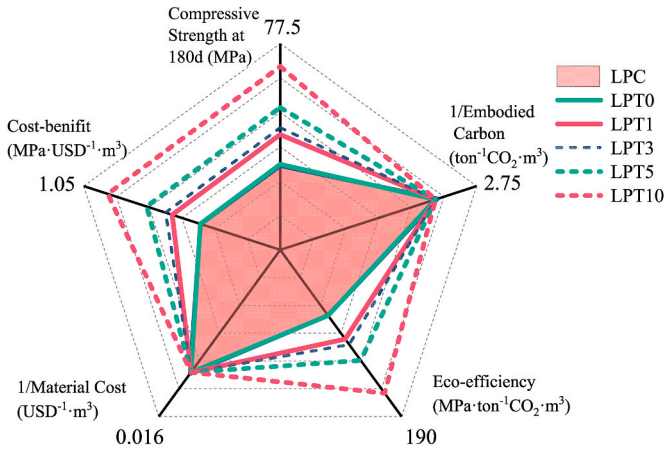

Fig. 13. Five-dimensinal assessment considering mechanical properties, embodied carbon, eco-efficiency, materials cost, and the cost benefit (strength per unit cost) of mortars with w/b of 0.45. The calculated embodied carbon and materials cost are based on 1 m^3 of mortars.

3.7. Practical implications of this study

The proposed method can make a direct contribution to the worldwide effort to reduce the carbon footprint generated by OPC based concretes. Typically, the carbon emission of the concrete is in proportion to the square root of its compressive strength. This study shows that 26% strength improvement can be reached by the proposed method, which is equivalent to reduce the carbon footprint of the concrete by 11%. An immediate application of the proposed method can be found on recycling returned fresh concrete waste and washing water in a concrete batching plant since these waste concrete and washing water are essentially the pre-hydrated cement slurries. After adding TA, they can be reused in the new mix of concrete to not only save cost associated with disposal of these wastes, but also improve the strength of the produced concrete.

It should be pointed out this study only evaluate the proposed method on the compressive strength of the concrete. It is still unclear how the proposed method can affect the long-term durability of the concrete. Theoretically, the durability of the cement mortars should be enhanced by using TA. This because TA can reduce the temperature rise at the early age and retain water during curing of the cement mortars. More importantly, TA is a well-known corrosion inhibitor and can enhance the corrosion resistance of steel embedded within the concrete. Further study is needed to confirm these speculations.

4. Conclusion

This study explores a pre-hydration process to mitigate the retarding effect of TA on the hydration of OPC so that TA can be used as a renewable admixture to improve the performance of concretes. Experimental results confirm that retarding effect of TA can be mitigated by the pre-carbonation method and drastic strength improvement can be achieved by the addition of TA. SEM and FTIR results revealed that nanoparticles can be in-situ produced by pre-hydrating a small amount of cement in the presence of TA. These nanoparticles can be well-dispersed in the slurry due to the steric impulsion generated by π-π stacking and function in the same way as externally added nanoparticles. The seeding effect of these nanoparticles significantly reduces the retarding effect of TA. The filler effect of the nanoparticles, together with the dispersion effect of TA densifies the microstructure of mortar, reduces the porosity of the samples up to 17.50%. Consequently, the nano-mechanical properties of hydration products are enhanced, as indicated by the improvement of elastic modulus and packing density by 16.05% and 2.98%, respectively. Similarly, the compressive strength at 180d can be increased up to 45%. This suggest that the eco-efficiency and cost-benefit of the cement mortars have been drastically improved by the proposed method, as confirmed by the economic and environmental analysis.

It should be pointed out that this study only confirms that the proposed method can enhance the compressive strength of the concrete. Future study will be carried out to examine the effect of the proposed method on the long-term durability of the concrete.

CRediT authorship contribution statement

Yi Fang: Methodology, Investigation, Visualization, Writing – original draft. **Jialai Wang:** Conceptualization, Funding acquisition, Supervision, Writing – review & editing. **Xin Qian:** Investigation. **Liang Wang:** Investigation. **Peiyuan Chen:** Investigation. **Pizhong Qiao:** Investigation, Supervision.

Declaration of competing interest

The authors declare that they have no known competing financial interests or personal relationships that could have appeared to influence the work reported in this paper.

Acknowledgements

This study was partially supported by the National Science Foundation, United States (CMMI – 1563551 and 1761672), Alabama Transportation Institute and the Fundamental Research Funds for the Central Universities at Tongji University (22120210131). Any opinions, findings, and conclusions or recommendations expressed in this material are those of the author(s) and do not necessarily reflect those of the National Science Foundation.

References

Abrams, D.A., 1920. Effect of Tannic Acid on the Strength of Concrete. Structural Research Laboratory. Lewis Institute, Chicago.
Arbenz, A., Avérous, L., 2015. Chemical modification of tannins to elaborate aromatic biobased macromolecular architectures. Green Chem. 17 (5), 2626–2646.
Arvanitoyannis, I.S., Ladas, D., Mavromatis, A., 2006. Potential uses and applications of treated wine waste: a review. Int. J. Food Sci. Technol. 41 (5), 475–487.
ASTM, 2008. ASTM C191-08: Standard Test Methods for Time of Setting of Hydraulic Cement by Vicat Needle. West Conshohocken, PA, pp. 1–14.
ASTM, 2015. ASTM C1437-15: Standard Test Method for Flow of Hydraulic Cement Mortar. West Conshohocken, PA.
ASTM, 2017. ASTM C1679 - 17: Standard Practices for Measuring Hydration Kinetics of Hydraulic Cementitious Mixtures Using Isothermal Calorimetry. West Conshohocken, PA, pp. 1–14.
ASTM, 2018a. ASTM C39/C39M-18: Standard Test Method for Compressive Strength of Cylindrical Concrete Specimens. West Conshohocken, PA.
ASTM, 2018b. C191-18a: Standard Test Methods for Time of Setting of Hydraulic Cement by Vicat Needle. West Conshohocken, PA.
Balasundram, N., Sundram, K., Samman, S., 2006. Phenolic compounds in plants and agri-industrial by-products: antioxidant activity, occurrence, and potential uses. Food Chem. 99 (1), 191–203.
Björnström, J., Martinelli, A., Matic, A., Börjesson, L., Panas, I., 2004. Accelerating effects of colloidal nano-silica for beneficial calcium–silicate–hydrate formation in cement. Chem. Phys. Lett. 392 (1–3), 242–248.
Çakar, S., Özacar, M., 2016. Fe–tannic acid complex dye as photo sensitizer for different morphological ZnO based DSSCs. Spectrochim. Acta Mol. Biomol. Spectrosc. 163, 79–88.
Chen, P., Zhang, L., Wang, Y., Fang, Y., Zhang, F., Xu, Y., 2021. Environmentally friendly utilization of coal gangue as aggregates for shotcrete used in the construction of coal mine tunnel. Case Stud. Construct. Mater., e00751
Damineli, B.L., Kemeid, F.M., Aguiar, P.S., John, V.M., 2010. Measuring the eco-efficiency of cement use. Cement Concr. Compos. 32 (8), 555–562.
Delgado, A.H., Paroli, R.M., Beaudoin, J.J., 1996. Comparison of IR techniques for the characterization of construction cement minerals and hydrated products. Appl. Spectrosc. 50 (8), 970–976.
Du, Y., Brumaud, C., Winnefeld, F., Lai, Y.-H., Habert, G., 2021. Mechanisms for efficient clay dispersing effect with tannins and sodium hydroxide. Colloid. Surface. Physicochem. Eng. Aspect. 127589.
Erel-Unal, I., Sukhishvili, S.A., 2008. Hydrogen-bonded multilayers of a neutral polymer and a polyphenol. Macromolecules 41 (11), 3962–3970.
Fang, Y., 2021. Low-cost, Ubiquitous Biomolecule as Next Generation, Sustainable Admixture to Enhance the Performance of Ordinary Portland Cement-Based Concretes. The University of Alabama, Ann Arbor, p. 212.
Fang, Y., Wang, J., Qian, X., Wang, L., Dong, Y., Qiao, P., 2021. Low-cost, ubiquitous biomolecule as a strength enhancer for cement mortars. Construct. Build. Mater. 311, 125305.
Flower, D.J., Sanjayan, J.G., 2007. Green house gas emissions due to concrete manufacture. Int. J. Life Cycle Assess. 12 (5), 282–288.
Guo, Z., Xie, W., Lu, J., Guo, X., Xu, J., Xu, W., Chi, Y., Takuya, N., Wu, H., Zhao, L., 2021. Tannic acid-based metal phenolic networks for bio-applications: a review. J. Mater. Chem. B. 9, 4098–4110.
Hansen, W., 1960. Actions of calcium sulfate and admixtures in Portland cement pastes. In: Symposium on Effect of Water-Reducing Admixtures and Set-Retarding Admixtures on Properties of Concrete. ASTM International.
Hughes, T.L., Methven, C.M., Jones, T.G., Pelham, S.E., Fletcher, P., Hall, C., 1995. Determining cement composition by Fourier transform infrared spectroscopy. Adv. Cement Base Mater. 2 (3), 91–104.
Iibuchi, S., Minoda, Y., Yamada, K., 1972. Hydrolyzing pathway, substrate specificity and inhibition of tannin acyl hydrolase of Asp. oryzae No. 7. Agric. Biol. Chem. 36 (9), 1553–1562.
Kajaste, R., Hurme, M., 2016. Cement industry greenhouse gas emissions–management options and abatement cost. J. Clean. Prod. 112, 4041–4052.
Kim, S., Pasc, A., 2017. Advances in multifunctional surface coating using metal-phenolic networks. Bull. Kor. Chem. Soc. 38 (5), 519–520.
Knapen, E., Van Gemert, D., 2009. Cement hydration and microstructure formation in the presence of water-soluble polymers. Cement Concr. Res. 39 (1), 6–13.
Lin, D., Xing, B., 2008. Tannic acid adsorption and its role for stabilizing carbon nanotube suspensions. Environ. Sci. Technol. 42 (16), 5917–5923.
Mondal, P., 2008. Nanomechanical Properties of Cementitious Materials. Northwestern University.
Oliver, W.C., Pharr, G.M., 1992. An improved technique for determining hardness and elastic modulus using load and displacement sensing indentation experiments. J. Mater. Res. 7 (6), 1564–1583.
Park, H., Jeong, Y., Jeong, J.-H., Oh, J.E., 2016. Strength development and hydration behavior of self-activation of commercial ground granulated blast-furnace slag mixed with purified water. Materials 9 (3), 185.
Pellenq, R.J.-M., Kushima, A., Shahsavari, R., Van Vliet, K.J., Buehler, M.J., Yip, S., Ulm, F.-J., 2009. A realistic molecular model of cement hydrates. Proc. Natl. Acad. Sci. Unit. States Am. 106 (38), 16102–16107.
Qian, X., Wang, J., Fang, Y., Wang, L., 2018. Carbon dioxide as an admixture for better performance of OPC-based concrete. J. CO2 Util. 25, 31–38.
Ren, Q., Zou, H., Liang, M., Wang, Y., Wang, J., 2014. Preparation and characterization of amphoteric polycarboxylate and the hydration mechanism study used in portland cement. RSC Adv. 4 (83), 44018–44025.
Ren, X., Yin, P., Liang, J., Liu, X., Zhan, W., Niu, J., Si, T., Yu, T., Wu, D., Wang, B., 2021. Insight into the tannic acid-based modular-assembly strategy based on inorganic–biological hybrid systems: a material suitability, loading effect, and biocompatibility study. Mater. Chem. Front. 5 (10), 3867–3876.
Rupasinghe, M., San Nicolas, R., Mendis, P., Sofi, M., Ngo, T., 2017. Investigation of strength and hydration characteristics in nano-silica incorporated cement paste. Cement Concr. Compos. 80, 17–30.
San Michele Mondovì, S.G., Gotti, Massimo, 2016. The Carbon Footprint in Leather Chemicals, World Leather. World Trades Publishing.
Shutava, T., Prouty, M., Kommireddy, D., Lvov, Y., 2005. pH responsive decomposable layer-by-layer nanofilms and capsules on the basis of tannic acid. Macromolecules 38 (7), 2850–2858.
Singh, L., Karade, S., Bhattacharyya, S., Yousuf, M., Ahalawat, S., 2013. Beneficial role of nanosilica in cement based materials–A review. Construct. Build. Mater. 47, 1069–1077.
Tennis, P.D., Jennings, H.M., 2000. A model for two types of calcium silicate hydrate in the microstructure of Portland cement pastes. Cement Concr. Res. 30 (6), 855–863.
Tuinukuafe, A.A., 2019. Nanostructural Characterization of Geopolymers. University of Alabama Libraries.
Turner, L.K., Collins, F.G., 2013. Carbon dioxide equivalent (CO2-e) emissions: a comparison between geopolymer and OPC cement concrete. Construct. Build. Mater. 43, 125–130.
Vandamme, M., Ulm, F., 2008. The Nanogranular Origin of Concrete Creep: a Nanoindentation Investigation of Microstructure and Fundamental Properties of Calcium-Silicate-Hydrates.
Vandamme, M., Ulm, F., 2013. Nanoindentation investigation of creep properties of calcium silicate hydrates. Cement Concr. Res. 52, 38–52.
Wang, L., Wang, J., Qian, X., Fang, Y., Chen, P., Tuinukuafe, A., 2020. Tea stain-inspired treatment for fine recycled concrete aggregates. Construct. Build. Mater. 262, 120027.
Yan, Y., Ouzia, A., Yu, C., Liu, J., Scrivener, K.L., 2020. Effect of a novel starch-based temperature rise inhibitor on cement hydration and microstructure development. Cement Concr. Res. 129, 105961.
Yan, Y., Scrivener, K.L., Yu, C., Ouzia, A., Liu, J., 2021. Effect of a novel starch-based temperature rise inhibitor on cement hydration and microstructure development: the second peak study. Cement Concr. Res. 141, 106325.
Yu, J., Wu, H.-L., Leung, C.K., 2020. Feasibility of using ultrahigh-volume limestone-calcined clay blend to develop sustainable medium-strength Engineered Cementitious Composites (ECC). J. Clean. Prod. 262, 121343.
Zhang, D.-F., Ju, B.-Z., Zhang, S.-F., Yang, J.-Z., 2008. The study on the synthesis and action mechanism of starch succinate half ester as water-reducing agent with super retarding performance. Carbohydr. Polym. 71 (1), 80–84.